IEEE Access
Multidisciplinary | Rapid Review | Open Access Journal

Received August 3, 2021, accepted August 18, 2021, date of publication August 24, 2021, date of current version August 30, 2021.

Digital Object Identifier 10.1109/ACCESS.2021.3106949

Dual-Band Quad-Polarized Transmitarray for 5G Mm-Wave Application

LIN-HUI HE, YONG-LING BAN, AND GANG WU, (Member, IEEE)
School of Electronic Science and Engineering, University of Electronic Science and Technology of China, Chengdu 611731, China

Corresponding author: Yong-Ling Ban (byl@uestc.edu.cn)

This work was supported by the National Natural Science Foundation of China under Grant 61971098 and Grant U19A2055, and in part by the National Key Research and Development Project under Grant 2020YFB1805003.

ABSTRACT A dual-band quad-polarized transmitarray (TA) is designed in a common aperture operating at 25.9/39.8 GHz. Using narrow strip patches as cells, the 25.9 GHz cells are arranged in the ±45° direction, and the 39.8 GHz cells are arranged in the 0/90° direction in the formed square gap of the 25.9 GHz cells to realize a compact design with four polarization directions. In each band of 25.9/39.8 GHz, the proposed TA is dual-polarization designed. Measurements show that the expected beams can be achieved, and their 3 dB gain bandwidth covers almost all of the 5G bands n258 (24.25–27.5 GHz) and n260 (37–440 GHz). This TA has potential application value in 5G construction.

INDEX TERMS Dual-band, quad-polarized, mm-Wave, 5G, transmitarray.

I. INTRODUCTION

The function of transmitarrays (TAs) or reflectarrays (RAs) is to converge a divergent spherical wave into a plane wave by placing unit cells with different phase shifts at different positions on the plane. TAs and RAs [1]–[14] are both effective solutions to achieve high gain aperture antennas, but the TAs have no feed shielding effect, which is more convenient for installation and use. For the dual-band TA, the main challenge is to make the cells independently change the transmission phase in two bands with low transmission loss, but it has a wider application space. Most of the existing dual-band TAs [15]–[27] are single polarized, and only a few dual-band TAs [28]–[31] adopt a dual polarized design, but they are single polarized in each band. Therefore, it is significant to design a dual band TA, which has dual-polarization designed in each band.

The 5G bands n258 (24.25–27.5 GHz) and n260 (37–440 GHz) are used for 5G mm-wave communication, so it is meaningful to design a dual-band quad-polarized TA operating at 25.9 GHz and 39.8 GHz. In this paper, a dual-band quad-polarized TA is proposed with ±45° polarization at 25.9 GHz and 0/90° polarization at 39.8 GHz. The transmission cell used here is a narrow strip patch [31]. First, dual polarization is realized by interleaving the linear polarization cells, then similar higher band cells are placed between the gaps of the lower band cells, and finally, the interaction between the cells is adjusted. To make the best use of space, the lower band cells are tilted 45°, and the higher band cells are placed horizontally or vertically, which makes the design more compact. Because of the high frequency, the phase changes rapidly with the size, so the narrow side of the strip patch remains unchanged, and the size changes are reflected on the longer side. This kind of operation can reduce the influence of machining error and maximize the design of higher frequency cells under the same machining error.

The dual-band quad-polarized TA designed in this paper has a total of 1681 linear polarization units, including four polarization directions. The final experimental results show that each polarization direction has a good gain and cross polarization level performance.

The associate editor coordinating the review of this manuscript and approving it for publication was Tutku Karacolak.

II. CELL DESIGN

A. INITIAL CELL

To conveniently describe the polarization direction of the electric field, a schematic diagram of the dual-band quad-polarized TA is shown here, in which each polarization direction can be represented by the angle with the x-axis,

This work is licensed under a Creative Commons Attribution 4.0 License. For more information, see https://creativecommons.org/licenses/by/4.0/

as shown in Fig. 1. The initial cell of the TA is shown in Fig. 2. It is made up of two rectangular strips that are perpendicular to each other and printed on each side of two identical 0.508 mm-thick dielectric substrates (Rogers RO4350B, $\varepsilon_{r1} = 3.66$, $\tan\delta_1 = 0.0037$). The two rectangular strips are connected by a metalized via, and the two substrates are connected by a 0.1 mm-thick adhesive film (Rogers4450F, $\varepsilon_{r1} = 3.52$, $\tan\delta_1 = 0.0042$), with the floor in the middle. This kind of transmit cell has the function of polarization rotation, and this kind of polarization rotation cell has a wider passband than that of a nonrotation cell [31].

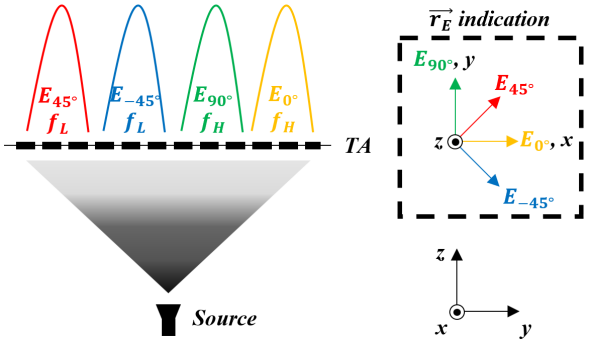

FIGURE 1. Schematic diagram of the dual-band quad-polarized TA.

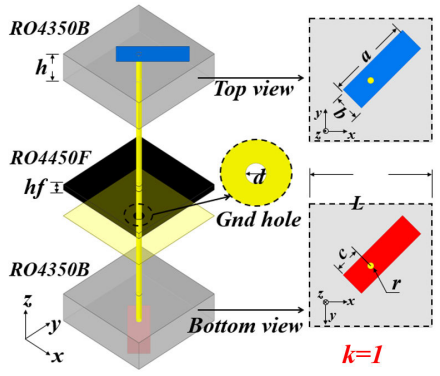

FIGURE 2. Initial cell design model.

B. DUAL-BAND QUAD-POLARIZED CELL

The −45°-pol cell is placed at the four corners of the 45°-pol cell, and a uniform dual-polarization array configuration can be formed [32]. Then, the 0° and 90° polarized patch cells are placed in the square space in the dual polarization array, and a dual-band quad-polarized array configuration can be formed. The formation process is shown in Fig. 3. The four different polarization linear polarization arrays share one aperture. The ±45°-pol cells are designed at 25.9 GHz, and 0°/90°-pol cells are designed at 39.8 GHz. The relationship between the polarization directions of ±45°, 0° and 90° and the coordinate axis is shown in Fig. 1.

The design model of a dual-band quad-polarized cell in the simulation software is shown in Fig. 4. Floquet ports and

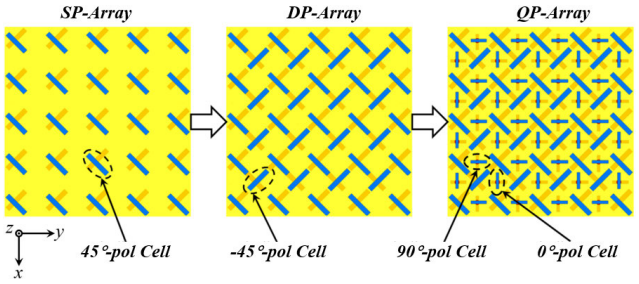

FIGURE 3. Formation process of dual bands and four polarizations.

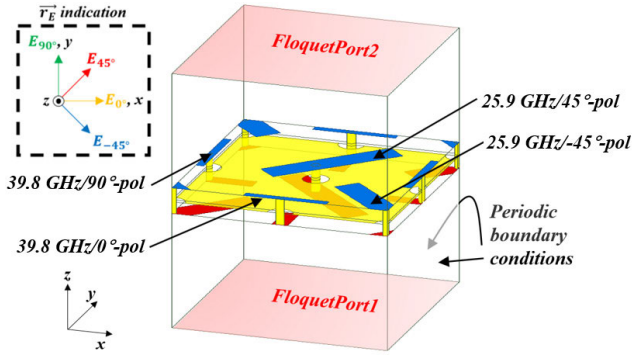

FIGURE 4. Design model of a dual-band quad-polarized cell.

periodic boundary conditions are used to simulate the cell. The parameter identification of the cell size is the same as in Fig. 2, and the specific design size is shown in Table 1. The coefficient $\boldsymbol{k}$ in Table 1 is used to define different sizes of cells. Furthermore, the coefficient $\boldsymbol{k}$ is mainly used to adjust the size of variables $\boldsymbol{a}$ and $\boldsymbol{c}$. Setting different $\boldsymbol{k}$ values can make the cell realize different phase responses. We set the value interval of $\boldsymbol{k}$ as 0.02 to ensure higher phase accuracy, so 16 different phases are used in first band and 8 different phases are used in second band. And due to the limited machining accuracy, it is meaningless to continue to reduce the value interval of $\boldsymbol{k}$.

TABLE 1. Design size of cell.

Symbol or variable	Lower band cell values	Higher band cell values
$\boldsymbol{k}$	0.93–1.07	0.58–0.64
$\boldsymbol{a}$	k×3.2 mm	k×3.2 mm
$\boldsymbol{b}$	0.6 mm	0.36 mm
$\boldsymbol{c}$	3a/8	9a/40
$\boldsymbol{r}$	0.1 mm	0.1 mm
$\boldsymbol{d}$	0.6 mm	0.6 mm
$\boldsymbol{h}$	0.508 mm	0.508 mm
$\boldsymbol{hf}$	0.101 mm	0.101 mm
$\boldsymbol{L}$	5 mm	5 mm

The value interval of variable $\boldsymbol{k}$ is 0.02.

Generally, the greater the distance between the two differently polarized cells, the better the cross-polarization transmission performance (since the transmission cell here

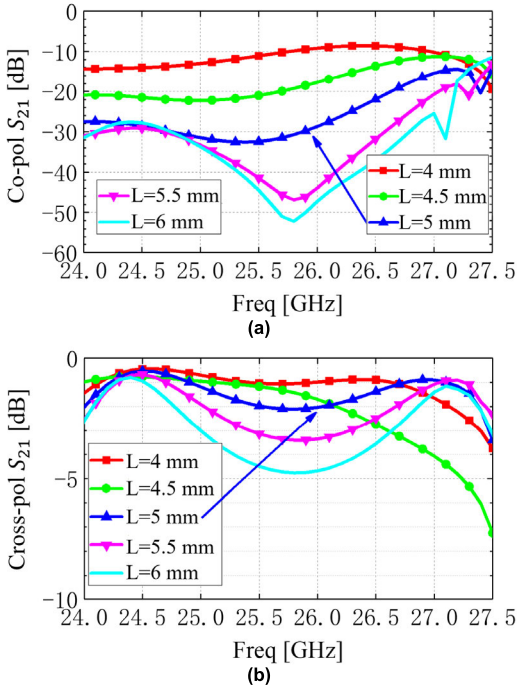

FIGURE 5. Relationship between the transmission S-parameter and L of 25.9 GHz cells: (a) Co-pol S_{21}, (b) Cross-pol S_{21}.

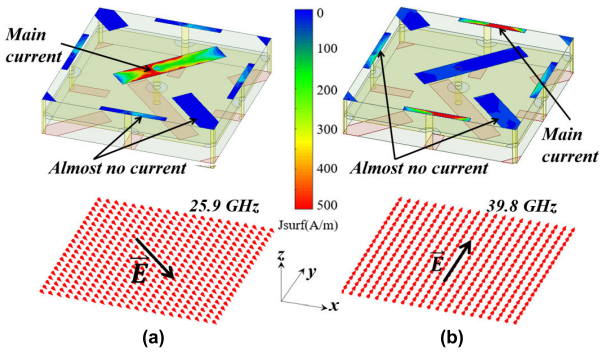

FIGURE 6. Current simulation of the dual-band quad-polarized cell: (a) 25.9 GHz excited, (b) 39.8 GHz excited.

has a 90° polarization rotation, homopolar transmission is unnecessary). The L is determined by scanning parameters. Fig. 5 shows the relationship between the transmission S-parameter and L of 25.9 GHz cells, and as L increases, the copolarized transmission S21 decreases. When L is 5 mm, the copolarized transmission S21 of 25.9 GHz cell is low, and when L continues to increase, the copolarized transmission S21 decreases slightly, but its cross-polarized transmission S21 decreases. Therefore, 5 mm is chosen as the distance between the cells for consideration of transmission performance and polarization isolation. The 39.8 GHz cells are farther apart in electrical length, so suppression of copolarized transmission should not be considered too much.

The current simulation of the dual-band quad-polarized cell is shown in Fig. 6. When the 25.9 GHz or 39.8 GHz cell is excited separately, there is almost no current in the uninspired cell with different frequencies or polarizations. Therefore, the linearly polarized cells placed in this way have little influence on each other, and the cells are very independent.

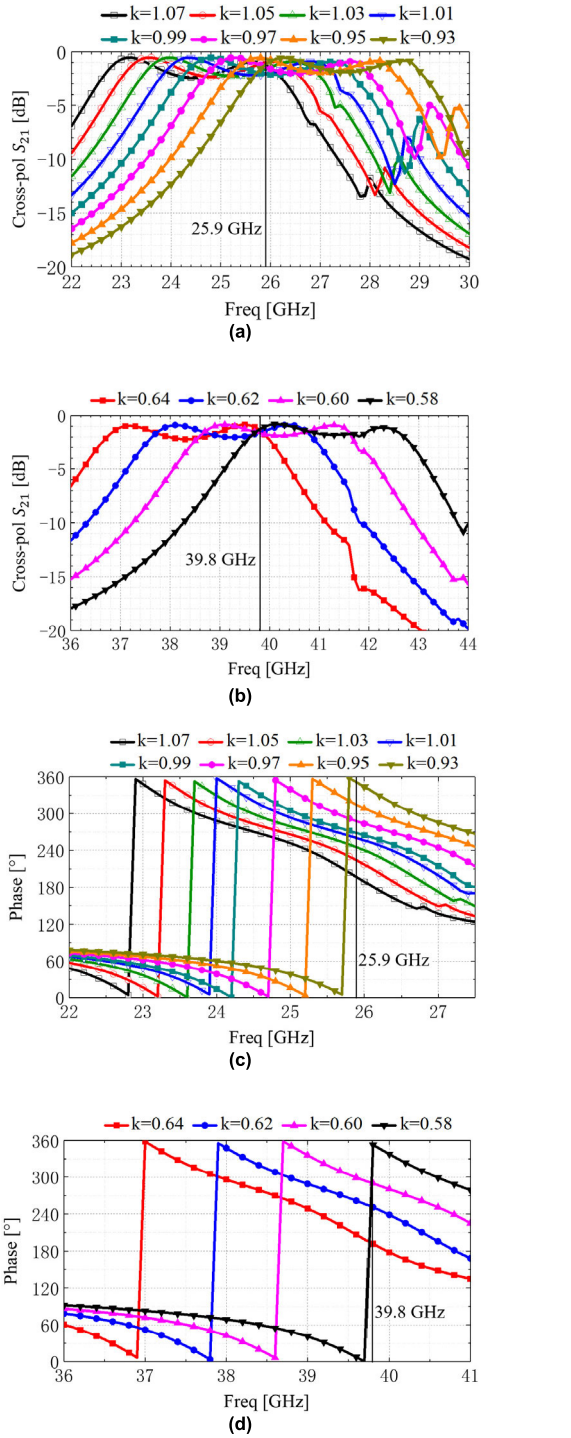

FIGURE 7. Cell characteristics: (a) 25.9 GHz amplitude-frequency characteristic curve, (b) 39.8 GHz amplitude-frequency characteristic curve, (c) 25.9 GHz phase-frequency characteristic curve, and (d) 39.8 GHz phase-frequency characteristic curve.

C. CELL CHARACTERISTICS: AMPLITUDE AND PHASE

This cell can obtain different phase responses by fine-tuning its size. The strip patch at the receiving end can be

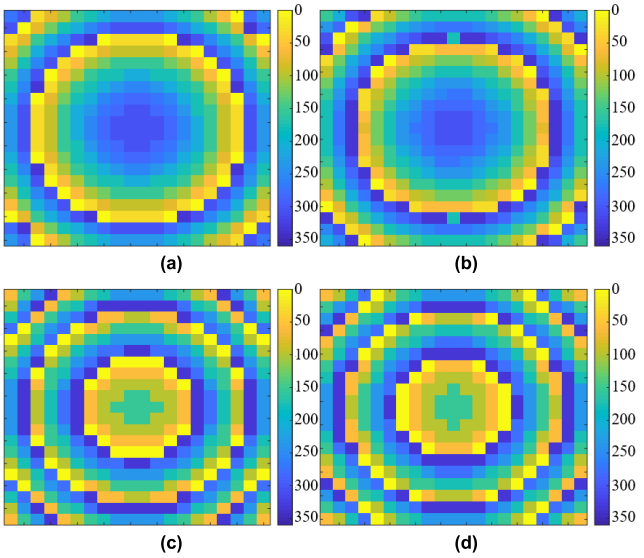

FIGURE 8. Phase surface extraction: (a) 25.9 GHz/−45°-pol, (b) 25.9 GHz/45°-pol, (c) 39.8 GHz/0°-pol, and (d) 39.8 GHz/90°-pol.

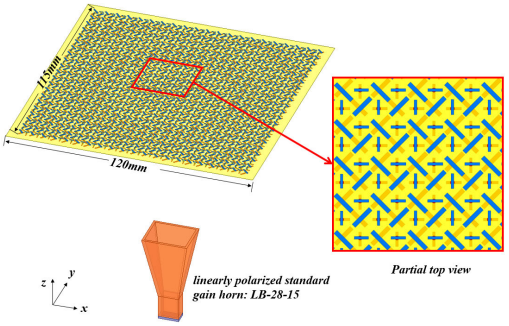

FIGURE 9. Design model of dual-band quad-polarized TA.

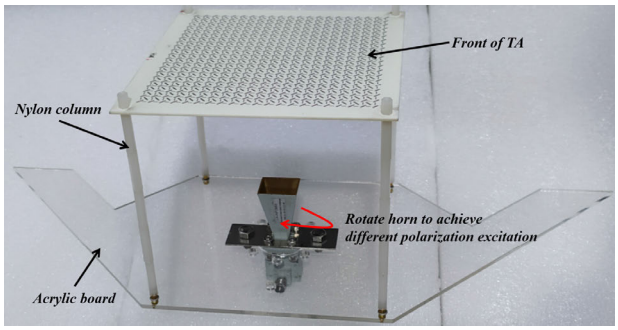

FIGURE 10. Physical model of dual-band quad-polarized TA.

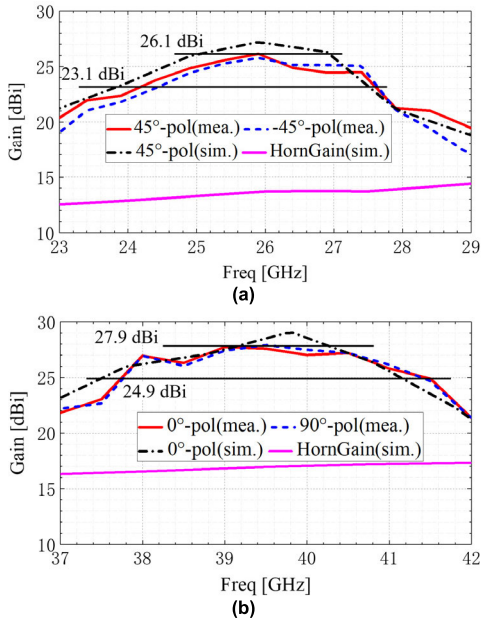

FIGURE 11. Gain test results of proposed TA: (a) Lower band, (b) Higher band.

symmetrically designed to achieve 0° and 180° phase shifts, so the cell only needs to meet the phase-shifting range of 0° to 180° when tuning the size. In addition, 360° phase coverage can be achieved through mirror symmetry. Considering the problem of processing accuracy, the value spacing of k in Table 1 is set to 0.02, that is, the minimum change in size is 2.5 mil length. Designed at 25.9 GHz is 4-bit cells with k ranging from 0.93 to 1.07. Since 39.8 GHz cells are smaller in size, 3-bit cells are designed at 39.8 GHz, with k ranging from 0.58 to 0.64.

The amplitude-frequency response of the cells is shown in Fig. 7(a) and (b). The −3 dB transmission bandwidth of a single cell is approximately 3.6 GHz but shared by all 25.9 GHz cells is only 1.4 GHz and by all 39.8 GHz cells is only 1.3 GHz. In a very wide bandwidth, more than half of the cells have an interpolation loss between 0 dB and 2 dB, which can greatly reduce the average transmission loss, so the total gain bandwidth is wider when designing arrays. Fig. 7(c) and (d) are phase-frequency response curves. The phase values are normalized to 0–360°. There are 8 different cells at 25.9 GHz and 4 different cells

TABLE 2. Phase-shift for different size cells.

cell	#1	#2	#3	#4	#5	#6	#7	#8
phase	351	314	287	268	259	245	224	196
cell	#9	#10	#11	#12	#13	#14	#15	#16
phase	171	134	107	88	79	65	44	16
cell	*1	*2	*3	*4	*5	*6	*7	*8
phase	353	290	251	192	173	110	71	12

at 39.8 GHz, and the total phase shift range of all cells covers almost 0–180°. Since this kind of cell has a 1-bit response at a fixed size, it can achieve a 0° or 180° response by mirroring itself symmetrically, so the original cells plus the symmetrically operated cells can cover almost 1–360°. Their respective simulation phase shifts are shown in Table 2, where the cells with coefficients $\boldsymbol{k}$ between 0.93 and 1.07 are defined as #1∼#8 (25.9 GHz cells) and the symmetrically operated cells are #9∼#16. The cells with $\boldsymbol{k}$ between 0.58 and 0.64 are defined as ∗1 ∼ ∗4 (39.8 GHz cells), and the symmetrically operated cells are ∗5 ∼ ∗8.

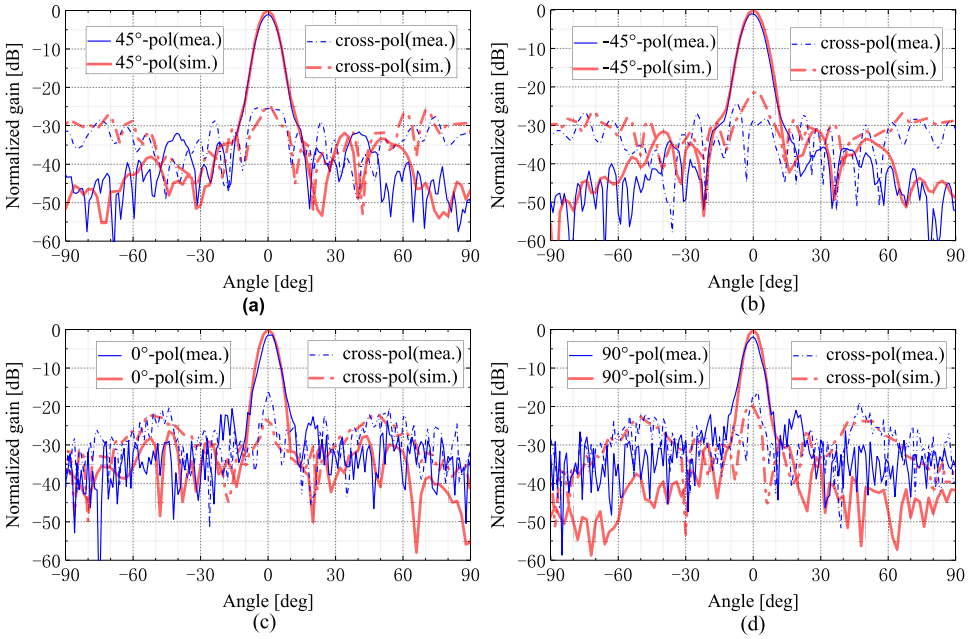

FIGURE 12. E-plane Pattern test results of dual-band quad-polarized TA: (a) 25.9 GHz/45°-pol, (b) 25.9 GHz/−45°-pol, (c) 39.8 GHz/0°-pol, and (d) 39.8 GHz/90°-pol.

III. TRANSMITARRAY

A. PHASE SURFACE EXTRACTION

When the antenna is fed by the horn, it is necessary to know the phase value received by each cell at each position of the array to determine the phase shift to be compensated. Therefore, it is necessary to extract the radiated electric field phase of the horn on the receiving surface of the array. To irradiate the radiation energy of the horn on the receiving surface of the array as much as possible, the F/D is 0.69. The horn selected here is a linear polarization standard gain horn lb-28-15 working in the Ka-band. Because the position of each polarization cell is different, the phase plane of each linear polarization array needs to be extracted separately. A total of four phase planes need to be extracted, as shown in Fig. 8, and the phase extraction value of each grid point is quantized according to the phase in Table 2.

B. SIMULATIONS AND MEASUREMENTS OF THE TA

The dual-band quad-polarized TA prototype is simulated and tested. The feed used here is a linear polarization standard gain horn lb-28–15. Because the test band is wide, we divided the frequency into several segments for calibration and testing. The array has 20 × 20 cells at 25.9 GHz/−45°-pol, 21 × 21 cells at 25.9 GHz/45°-pol, 20 × 21 cells at 39.8 GHz/0°-pol and 21 × 20 cells at 39.8 GHz/90°-pol. A total of 1681 linearly polarized cells were arranged alternately. The design model of the dual-band quad-polarized TA is shown in Fig. 9. The size of the substrate is 120 mm × 120 mm, and the area of radiation cells is 105 mm × 105 mm. Four linearly polarized arrays are excited by changing the excitation frequency and rotating direction of the horn.

To reduce the influence of the fixing device, an acrylic plate and nylon column are used to fix the TA. The physical model of the dual-band quad-polarized TA is shown in Fig. 10. The feed horn is fixed on the acrylic plate by bolts, and there are fixing holes to allow the horn to rotate on the acrylic plate. Here, only four central beams are simulated and tested, and the gain and pattern test results are shown in Fig. 11 and Fig. 12. Because the array is large and difficult to simulate, only one polarization is simulated at each band.

The test results show that the peak gain is 26.1 dBi/45°-pol and 25.8/−45°-pol in the lower band (23–229 GHz), which is approximately 1 dB lower than the simulation result (27.1/26.8 dBi), and its 3 dB gain bandwidth is approximately 24.2–27.6 GHz. The peak gain of 27.9 dBi in the higher band (37–442 GHz) is 1.2 dB lower than that of the simulation result (29.1 dBi), and its 3 dB gain bandwidth is approximately 37.7–41.5 GHz. The pattern in Fig. 12 is normalized with the simulated gain as a reference. The tested and simulated patterns have the same ascending and descending trend from 0° to 90°, and all sidelobes and cross-polarization levels tested are below −17 dB on average. The higher the angle is, the higher the cross-polarization level is. This is caused by the polarization rotation in the transmission cells. The polarization direction of the horn is the cross-polarization direction of the array. Therefore, when the horn radiates at a large angle, the gain overflows the array, which causes the cross-polarization level to become higher.

Taking 105 mm × 105 mm as the aperture size of the array, according to the test results, the actual aperture efficiency of the dual-band quad-polarized TA is 39.4%/45°-pol, 36.8%/−45°-pol at 25.9 GHz, and 25.3% at 39.8 GHz

TABLE 3. Comparison of dual-band TA.

Ref	Freq(GHz)	Gain(dBi)	3 dB-Gain band(%)	Polarization	F/D	Aperture efficiency(%)
[25]	12 18	27.8 31.4	3.3 3.4	SL	0.8	52 53
[26]	20 30	15.3 15.3	10 7	SC	0.69	10 6
[27]	12 14.2	23.9 24.5	7.5 7	DC	0.65	32.2 28.9
[28]	11 12.5	23.6 24.4	6.8 5.4	DL	0.8	38 34.6
[29]	19.8 29.1	21.4 23.4	19.8 12	DL	0.6	25.1 25
[30]	12.5 14.3	31 31.8	7.2 7	DL	0.75	45 41
[31]	20 30	29.0 25.9	11.3 11.4	DL	0.6	20.1 21.2
This work	**25.9** **39.8**	**26.1|25.8** **27.9**	**13.1|12.7** **9.6**	**FL**	**0.69**	**39.4|36.8** **25.3**

Here, SL is single line polarization, SC is single circle polarization, DC is dual circle polarization, DL is dual line polarization and FL is four line polarization

because of the large spacing of the higher band cells. Table 3 shows the parameter comparison between some existing dual-band transmission arrays and the proposed TA. Compared with the dual-band or dual-polarized transmission array, the array designed in this paper is not inferior in aperture efficiency, polarization purity, array size, gain bandwidth, and other parameters. Moreover, dual-polarization transmission is realized in each band, which is a highlight of this design.

IV. CONCLUSION

Using the common radiation aperture method, a dual-band quad-polarized TA operating at 25.9/39.8 GHz is presented. The 3 dB gain bandwidth can almost cover all of the 5G bands n258 (24.25–27.5 GHz) and n260 (37–40 GHz). It has been proven that the proposed TA can achieve good beam convergence and polarization independence at each polarization and can be used for 5G millimeter-wave applications.

REFERENCES

[1] Y. Hu, W. Hong, and Z. H. Jiang, "A multibeam folded reflectarray antenna with wide coverage and integrated primary sources for millimeter-wave massive MIMO applications," *IEEE Trans. Antennas Propag.*, vol. 66, no. 12, pp. 6875–6882, Dec. 2018.

[2] W. Li, S. Gao, L. Zhang, Q. Luo, and Y. Cai, "An ultra-wide-band tightly coupled dipole reflectarray antenna," *IEEE Trans. Antennas Propag.*, vol. 66, no. 2, pp. 533–540, Feb. 2018.

[3] C. G. M. Ryan, M. R. Chaharmir, J. Shaker, J. R. Bray, Y. M. M. Antar, and A. Ittipiboon, "A wideband transmitarray using dual-resonant double square rings," *IEEE Trans. Antennas Propag.*, vol. 58, no. 5, pp. 1486–1493, May 2010.

[4] J. Y. Lau and S. V. Hum, "A wideband reconfigurable transmitarray element," *IEEE Trans. Antennas Propag.*, vol. 60, no. 3, pp. 1303–1311, Mar. 2012.

[5] B. Rahmati and H. R. Hassani, "High-efficient wideband slot transmitarray antenna," *IEEE Trans. Antennas Propag.*, vol. 63, no. 11, pp. 5149–5155, Nov. 2015.

[6] K. Pham, N. T. Nguyen, A. Clemente, L. Di Palma, L. L. Coq, L. Dussopt, and R. Sauleau, "Design of wideband dual linearly polarized transmitarray antennas," *IEEE Trans. Antennas Propag.*, vol. 64, no. 5, pp. 2022–2026, May 2016.

[7] W. An, S. Xu, F. Yang, and M. Li, "A double-layer transmitarray antenna using Malta crosses with vias," *IEEE Trans. Antennas Propag.*, vol. 64, no. 3, pp. 1120–1125, Mar. 2016.

[8] Y. Hou, L. Chang, Y. Li, Z. Zhang, and Z. Feng, "Linear multibeam transmitarray based on the sliding aperture technique," *IEEE Trans. Antennas Propag.*, vol. 66, no. 8, pp. 3948–3958, Aug. 2018.

[9] K. Mavrakakis, H. Luyen, J. H. Booske, and N. Behdad, "Wideband transmitarrays based on polarization- rotating miniaturized-element frequency selective surfaces," *IEEE Trans. Antennas Propag.*, vol. 68, no. 3, pp. 2128–2137, Mar. 2020.

[10] T. Li and Z. N. Chen, "Compact wideband wide-angle polarization-free metasurface lens antenna array for multibeam base stations," *IEEE Trans. Antennas Propag.*, vol. 68, no. 3, pp. 1378–1388, Mar. 2020.

[11] X. Liu, L. Peng, Y.-F. Liu, W.-S. Yu, Q.-X. Zhao, X. Jiang, S.-M. Li, and C. Ruan, "Ultrabroadband all-dielectric transmitarray designing based on genetic algorithm optimization and 3-D print technology," *IEEE Trans. Antennas Propag.*, vol. 69, no. 4, pp. 2003–2012, Apr. 2021.

[12] K. K. Katare, S. Chandravanshi, A. Sharma, A. Biswas, and M. J. Akhtar, "Anisotropic metasurface-based beam-scanning dual-polarized fan-beam integrated antenna system," *IEEE Trans. Antennas Propag.*, vol. 67, no. 12, pp. 7204–7215, Dec. 2019.

[13] C. Fan, W. Che, W. Yang, and S. He, "A novel PRAMC-based ultralow-profile transmitarray antenna by using ray tracing principle," *IEEE Trans. Antennas Propag.*, vol. 65, no. 4, pp. 1779–1787, Apr. 2017.

[14] Y.-M. Cai, W. Li, K. Li, S. Gao, Y. Yin, L. Zhao, and W. Hu, "A novel ultra-wideband transmitarray design using tightly coupled dipole elements," *IEEE Trans. Antennas Propag.*, vol. 67, no. 1, pp. 242–250, Jan. 2019.

[15] Z. Zhang, X. Li, C. Sun, Y. Liu, and G. Han, "Dual-band focused transmitarray antenna for microwave measurements," *IEEE Access*, vol. 8, pp. 100337–100345, 2020.

[16] K. Pham, R. Sauleau, E. Fourn, F. Diaby, A. Clemente, and L. Dussopt, "Dual-band dual-polarized transmitarrays at Ka-band," in *Proc. Eur. Conf. Antennas Propag.*, Paris, France, Mar. 2017, pp. 59–62.

[17] P. Mei, S. Zhang, and G. F. Pedersen, "A dual-polarized and high-gain X-/Ka-band shared-aperture antenna with high aperture reuse efficiency," *IEEE Trans. Antennas Propag.*, vol. 69, no. 3, pp. 1334–1344, Mar. 2021.

[18] A. Aziz, F. Yang, S. Xu, and M. Li, "Design of a dual-band orthogonally polarized transmitarray using 3-dipole elements," in *Proc. Asia–Pacific Conf. Antennas Propag.*, Xi'an, China, Oct. 2017, pp. 1–3.

[19] A. Aziz, F. Yang, S. Xu, M. Li, and H.-T. Chen, "A high-gain dual-band and dual-polarized transmitarray using novel loop elements," *IEEE Antennas Wireless Propag. Lett.*, vol. 18, no. 6, pp. 1213–1217, Jun. 2019.

[20] K. Pham, R. Sauleau, E. Fourn, F. Diaby, A. Clemente, and L. Dussopt, "K/Ka-band transmitarray antennas based on polarization twisted unit-cells," in *Proc. Eur. Conf. Antennas Propag.*, London, U.K., 2018, pp. 1–5.

[21] M. R. Chaharmir, A. Ittipiboon, and J. Shaker, "Single-band and dual-band multilayer transmitarray antennas," in *Proc. Int. Symp. Antenna Techn. Appl. Electromagn. Can. Radio Sci. Conf.*, Montreal, QC, Canada, 2006, pp. 1–4.

[22] T. K. Pham, L. Guang, D. González-Ovejero, and R. Sauleau, "Dual-band transmitarray with low scan loss for satcom applications," *IEEE Trans. Antennas Propag.*, vol. 69, no. 3, pp. 1775–1780, Mar. 2021.
[23] S. Yang, Z. Yan, T. Zhang, M. Cai, F. Fan, and X. Li, "Multifunctional tri-band dual-polarized antenna combining transmitarray and reflectarray," *IEEE Trans. Antennas Propag.*, early access, Feb. 26, 2021, doi: 10.1109/TAP.2021.3060938.
[24] A. Aziz, X. Zhang, F. Yang, S. Xu, and M. Li, "A dual-band orthogonally polarized contour beam transmitarray design," *IEEE Trans. Antennas Propag.*, vol. 69, no. 8, pp. 4538–4545, Aug. 2021.
[25] R. Y. Wu, Y. B. Li, W. Wu, C. B. Shi, and T. J. Cui, "High-gain dual-band transmitarray," *IEEE Trans. Antennas Propag.*, vol. 65, no. 7, pp. 3481–3488, Jul. 2017.
[26] H. Hasani, J. S. Silva, S. Capdevila, M. García-Vigueras, and J. R. Mosig, "Dual-band circularly polarized transmitarray antenna for satellite communications at (20, 30) GHz," *IEEE Trans. Antennas Propag.*, vol. 67, no. 8, pp. 5325–5333, Aug. 2019.
[27] Y.-M. Cai, K. Li, W. Li, S. Gao, Y. Yin, L. Zhao, and W. Hu, "Dual-band circularly polarized transmitarray with single linearly polarized feed," *IEEE Trans. Antennas Propag.*, vol. 68, no. 6, pp. 5015–5020, Jun. 2020.
[28] M. O. Bagheri, H. R. Hassani, and B. Rahmati, "Dual-band, dual-polarised metallic slot transmitarray antenna," *IET Microw., Antennas Propag.*, vol. 11, no. 3, pp. 402–409, 2017.
[29] R. Madi, A. Clemente, and R. Sauleau, "Dual-band dual-linearly polarized transmitarray at Ka-band," in *Proc. Eur. Microw. Conf.*, Utrecht, The Netherlands, Jan. 2021, pp. 340–343.
[30] A. Aziz, F. Yang, S. Xu, and M. Li, "An efficient dual-band orthogonally polarized transmitarray design using three-dipole elements," *IEEE Antennas Wireless Propag. Lett.*, vol. 17, no. 2, pp. 319–322, Feb. 2018.
[31] K. T. Pham, R. Sauleau, E. Fourn, F. Diaby, A. Clemente, and L. Dussopt, "Dual-band transmitarrays with dual-linear polarization at Ka-band," *IEEE Trans. Antennas Propag.*, vol. 65, no. 12, pp. 7009–7018, Dec. 2017.
[32] K. T. Pham, A. Clemente, D. Blanco, and R. Sauleau, "Dual-circularly polarized high-gain transmitarray antennas at *Ka*-band," *IEEE Trans. Antennas Propag.*, vol. 68, no. 10, pp. 7223–7227, Oct. 2020.

LIN-HUI HE was born in Sichuan, China, in 1995. He received the B.S. degree in electronic science and technology from Chongqing University of Posts and Telecommunications, Chongqing, China, in 2018. He is currently pursuing the M.S. degree in electronic and communication engineering with the University of Electronic Science and Technology of China (UESTC), Chengdu, China. His current research interests include dual-polarized multibeam antennas and arrays.

YONG-LING BAN was born in Henan, China. He received the B.S. degree from the School of Mathematics, Shandong University, the M.S. degree from the School of Information Science and Technology, Peking University, and the Ph.D. degree from the School of Electronic Engineering, University of Electronic Science and Technology of China (UESTC), in 2000, 2003, and 2006, respectively.

In July 2006, he joined Xi'an Mechanical and Electric Information Institute, as a Microwave Engineer. He then joined Huawei Technologies Company Ltd., Shenzhen, China. At Huawei, he designed and implemented various terminal antennas for 15 data card and mobile phone products customized from leading telecommunication industries like Vodafone. From September 2010 to July 2016, he was an Associate Professor with UESTC and promoted to a Professor, in 2016. From May 2014 to April 2015, he visited Queen Mary University of London, as a Scholar Visitor. In 2020, he was selected into UESTC's 100 Talents Program and selected into Elsevier 2020 Most Cited Chinese Researchers. Since 2012, he has been publishing more than 100 SCI journal articles, including five ESI highly cited articles, and applied for 30 patents at home and abroad, of which more than 20 are authorized. His current research interests include 5G/6G microwave/millimeter wave antenna and array, phased metasurface antenna array, lens antenna, RCS backward enhancement structure and technology. He received two second prizes at the Provincial and Ministerial Level. In addition, he has presided over more than 20 projects, such as NSFC and enterprise cooperation. He has been a TPC member of international academic conferences for many times, and reviewed manuscripts for IEEE Transactions on Antennas and Propagation and IEEE Antennas and Wireless Propagation Letters.

GANG WU (Member, IEEE) received the B.S. and M.S. degrees in radio communications engineering from Chongqing University of Post and Telecommunications, Chongqing, China, in 1996 and 1999, respectively, and the Ph.D. degree in communications and information systems from the University of Electronic Science and Technology of China (UESTC), Chengdu, China, in 2004.

In June 2004, he joined UESTC, as a Lecturer. He was a Research Fellow with the Positioning and Wireless Technology Centre, Nanyang Technological University, Singapore, from November 2005 to February 2007, and a Visiting Scholar with Georgia Institute of Technology, Atlanta, GA, USA, from September 2009 to September 2010. He is currently a Professor with the National Key Laboratory of Science and Technology on Communications, UESTC. His research interests include MIMO-OFDM, cooperative communications, cognitive radio, resource allocation and scheduling for wireless networks, and energy-efficient wireless networks. He was awarded as an Exemplary Reviewer of IEEE Communications Letters, in 2011, and received the IEEE Globecom 2012 Best Paper Award. He served as a technical reviewer of dozens of international journals and conferences. He has also been a technical program committee member of several international conferences.